Response analysis of soil deposit considering both frequency and strain amplitude dependencies using nonlinear causal hysteretic damping model

Naohiro Nakamura[*]

Research & Development Institute, Takenaka Corporation, 1-5-1, Ohtsuka, Inzai, Chiba, Japan, 270-1395

Abstract. It is well known that the properties of the soil deposits, especially the damping, depend on both frequency and strain amplitude. Therefore it is important to consider both dependencies to calculate the soil response against earthquakes in order to estimate input motions to buildings. However, it has been difficult to calculate the seismic response of the soil considering both dependencies directly. The author has studied the time domain evaluation of the frequency dependent dynamic stiffness, and proposed a simple hysteretic damping model that satisfies the causality condition. In this paper, this model was applied to nonlinear analyses considering the effects of the strain amplitude dependency of the soil. The basic characteristics of the proposed method were studied using a two layered soil model. The response behavior was compared with the conventional model e.g. the Ramberg-Osgood model and the SHAKE model. The characteristics of the proposed model were studied with regard to the effects of element divisions and the frequency dependency that is a key feature of the model. The efficiency of the model was confirmed by these studies.

Keywords: frequency dependency; strain dependency; soil response; hysteretic damping; nonlinear analysis

1. Introduction

Earthquake ground motions that input to buildings are greatly affected by the amplification characteristics of the surface soil layer. Therefore, in order to estimate the behavior of the buildings during severe earthquakes, it is essential to appropriately evaluate the amplification characteristics. Although investigations have been carried out, many problems at present remain unsolved with regard to the characteristics, especially the damping property (e.g. Kausel *et al.* 2002, Yoshida *et al.* 2002, Kumasaki *et al.* 1998).

It is well known that soil shows strong nonlinear behavior during an earthquake and the dynamic characteristics of the soil vary depending on the strain amplitude. It is also indicated that the material damping of the soil is almost independent of the frequency. In contrast, some studies (e.g. Yoshida *et al.* 2002) indicate that the damping ratio of the soil deposit tends to decrease with an increase in the frequency. In both cases, it is important to consider the frequency dependency of

---

[*]Corresponding author, Ph. D., E-mail: nakamura.naohiro@takenaka.co.jp

the soil damping. Because the frequency non-dependency is a special case of the frequency dependency, it is often very difficult to express the frequency non-dependency of the damping in the time domain analysis. Therefore, it is necessary to take into account both the frequency dependency and the strain dependency (hereafter referred to as both dependencies) in accurately modeling the damping characteristics of the soil.

For this purpose, equivalent linear analysis methods such as SHAKE (Schnabel *et al.* 1972) or methods obtained by improving this model (e.g. Sato *et al.* 2001) are often used. However, it is indicated that the accuracy of the results from these methods is not good when the strain level of the soil is large. Alternatively, time history response analysis methods are often used. These methods use a skeleton curve that varies depending on the strain level and the hysteresis rule such as the Masing rule (Masing 1926) or an improvement of this rule, namely, the Ramberg-Osgood model (Jennings 1963) (hereafter referred to as the R-O model) and the hyperbolic model (Hardin *et al.* 1972). These models are controlled by using the dynamic deformation characteristics that comprise the relation between the shear modulus degradation coefficient and the cyclic shear strain amplitude (G/G_0-γ) and the relation between the damping ratio and the aforementioned strain amplitude (h-γ).

In these models, it is impossible to control the frequency dependency directly. In addition, the dynamic deformation characteristics are limited by the definition of the models, so the characteristics obtained from experimental results cannot be directly applied.

Therefore, a nonlinear soil response analysis method that can directly control both dependencies and use the arbitrary dynamic deformation characteristics is needed.

The author has studied the transform methods of the frequency dependent dynamic stiffness to the time domain and the time history response analysis method using these transform methods (Nakamura 2006a, 2006b, 2008a). Then, a damping model that is causal and nearly frequency-independent (hereafter referred to as the causal hysteretic damping model) was proposed. The efficiency and the applicability of the model to the time history response analysis were confirmed (Nakamura 2007). Moreover, nonlinear time history response analyses of a building on layered soil considering the soil impedance whose frequency dependency varies depending on the strain level of the soil were studied (Nakamura 2008b). In this paper, first, a set of the frequency dependent soil impedances corresponding to each strain level was calculated. Then, a set of the impulse responses was obtained by transforming them to the time domain. The time history response analyses were carried out by changing the impulse response corresponding to the current strain level. However, both dependencies were considered for only two springs (sway and rocking components of impedance), and they were pre-calculated before the time history response analysis of the soil-structure interaction system.

In this paper, a method for analyzing the time history response of the soil is proposed based on the above studies using the nonlinear causal hysteretic damping model in which both dependencies are explicitly controlled. In this analysis, both dependencies are considered for many elements of the model. Therefore, the strain of each element is changing because of the dynamic deformation characteristics of each layer and affecting each other in the time history response analysis. The nonlinear causal hysteretic model is used to express these dependencies.

First, the outline of the causal hysteretic damping model is described and then the method for expanding the model to the nonlinear analysis is explained. Next, the response behavior of the proposed model is compared with the conventional R-O and SHAKE models. Then, the effects of the element division are also investigated.

Moreover, the control parameters used in this analysis are investigated. The key characteristic

of the proposed model is that the frequency dependency can be directly prescribed. Accordingly, the effects of this model upon the response are investigated using a model whose damping ratio varies depending on the frequency.

In fact, the nonlinearity of the soil is very complex and depends on many parameters such as vertical normal stress, particle size distribution, and over-consolidation ratio. In contrast, the proposed model is one of the simplest nonlinear models for the total stress analysis. As nonlinear properties, only the G/G_0-γ and the h-γ relation are considered under the condition of frequency dependency. Therefore, it can be said that the proposed model is the time domain version of SHAKE model. Accordingly, this model can be applied not only to soil problems but also any structural element.

2. Outline of the causal hysteretic damping model

It is well known that the damping ratios of many materials do not depend upon the frequency. A damping model having this property is called the hysteretic damping model.

In reality, the results follow the causes in time history and no phenomena occur otherwise. This is called "the causality law" and the state satisfying this condition is called "causal".

In the frequency region, the hysteretic damping can be easily indicated using a complex damping model. However, if this model is transformed to the time domain directly, it becomes non-causal (state in which the causality is broken) and cannot be used in the time history response analysis.

The proposed causal hysteretic damping model is able to approximately indicate the complex damping model in the time domain while satisfying causality.

The formulation of the causal hysteretic damping model as well as the outline of the method for nonlinearity is shown below. Details can be seen in (Nakamura 2008a).

2.1 Formulation of the causal hysteretic damping model

The complex stiffness including the hysteretic damping is described by Eqs. (1) and (2). $F(\omega)$ is the force and $u(\omega)$ is the displacement. The causal unit imaginary function $Z'(\omega)$ is applied in place of $\text{sgn}(\omega) \cdot i$ for the complex damping model $K_0(1 + 2h \cdot \text{sgn}(\omega) \cdot i)$ where K_0 is the initial stiffness of the problem, h is the damping ratio and i is the imaginary unit.

$$F(\omega) = S'(\omega) \cdot u(\omega) \tag{1}$$

where

$$S'(\omega) = K_0(1 + 2h) \cdot Z'(\omega) \tag{2}$$

The imaginary part of $Z'(\omega)$ is set as a function with an almost constant value (=1) in certain frequency ranges (hereafter referred to as the focused frequency ranges) $0 \sim \omega_m$. The upper limit of the range (ω_m) is defined by the user. The real part is set as a causal function calculated from the imaginary part using the Hilbert transform.

The transform of $Z'(\omega)$ to the time domain results in obtaining the impulse response with the simultaneous component of the damping term (c_0) and the stiffness term time delay components

$(k_1, k_2 \ldots k_n, k_j=k(\Delta t \cdot j))$, where Δt shows the time step.

The "simultaneous component" means the amount that causes the reaction depending on the present displacement and velocity. The "time delay component" implies the quantity that induces the reaction depending on the past displacement and velocity.

For $Z'(\omega)$, the simultaneous component of the stiffness term k_0 and the time delay components of the damping term $c_1, c_2, \ldots c_n$ become 0. From the above, $Z'(\omega)$ can be expressed by Eq. (3).

$$Z'(\omega) = i\omega \cdot c_0 + \sum_{j=1}^{n} k_j \cdot e^{-i\omega t_j} \tag{3}$$

The force in the time domain $F(t)$, corresponding to $F(\omega)$ in Eq. (1), can be shown by Eqs. (4) and (5) using the displacement $u(t)$ and the velocity $\dot{u}(t)$. $z'(t)$ is the value in the time domain that corresponds to $i \cdot u(\omega)$ in the frequency domain.

$$F(t) = K_0[u(t) + 2h \cdot z'(t)] \tag{4}$$

where

$$z'(t) = c_0 \cdot \dot{u}(t) + \sum_{j=1}^{n} k_j \cdot u(t - t_j) \tag{5}$$

In this paper, the focused frequency ranges are set to 0~10 Hz and the data points used in the transform are set at 9 points from 1 through 9 Hz. The transform to the time domain is carried out under the condition t=0.1sec. Fig. 1 shows the stiffness term of the obtained impulse response. The value of the simultaneous component of the damping term c_0 is $0.1/\pi$. Fig. 2 shows the impedance of the causal unit imaginary function reconstructed from the obtained impulse response using Eq. (3). The white circle marks in the Fig. show the original data points used in the transform. The reconstructed impedance corresponds well to the original data points, therefore it is confirmed that the accuracy of the transform is high.
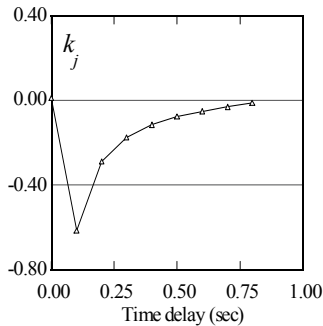
2.2 Outline of the method for nonlinearity

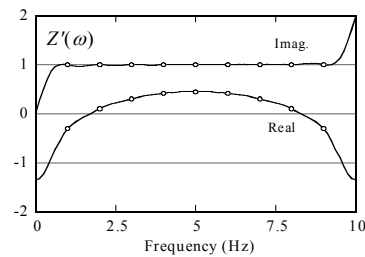Fig. 1 Impulse response of calculated causal unit imaginary function (stiffness term k_j)

Fig. 2 Reconstructed impedance of causal unit imaginary function $Z'(\omega)$

Further, the nonlinearity of the proposed model is considered. The case of $[K(\gamma_m, \omega)]_e$ in which the element stiffness matrix varies according to the dynamic deformation characteristics is shown in Eq. (6). $\alpha_e(\gamma_m)$ shows the stiffness degradation coefficient and has a similar meaning as G/G_0. $h_e(\gamma_m)$ shows the damping ratio of the corresponding element. These parameters depend on the maximum strain γ_m that is the maximum strain in the past t_m. In other words, t_m is the memory time of shear strain. Its effect of is studied in section 4.2. $[K_0]_e$ indicates the initial element stiffness matrix.

$$\left[K(\gamma_m, \omega)\right]_e = \alpha_e(\gamma_m)\left[K_0\right]_e(1 + 2h_e(\gamma_m) \cdot Z'(\omega)) \tag{6}$$

This element reaction vector in the time domain $\{F(\gamma_m, t)\}_e$ can be indicated as Eq. (7). $\{u(t)\}_e$ is the displacement vector and $t_j = j\Delta t$.

$$\{F(\gamma_m, t)\}_e = \left[K_0\right]_e \alpha_e(\gamma_m)\left(\{u_e(t)\} + 2h_e(\gamma_m)c_0\{\dot{u}_e(t)\}\right) + 2\left[K_0\right]_e \sum_{j=1}^{n} \alpha_e(\gamma_m)h_e(\gamma_m)k_j \cdot \{u_e(t - t_j)\} \tag{7}$$

3. Study of the applicability to multi degree of freedom system model

In order to study the applicability of the proposed model relative to the conventional models,

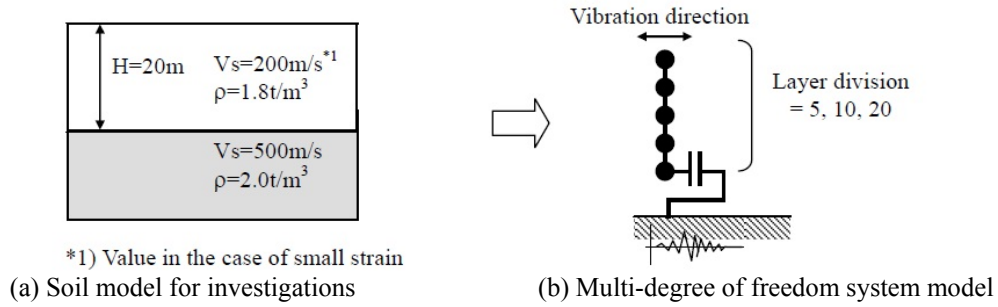(a) Soil model for investigations   (b) Multi-degree of freedom system model
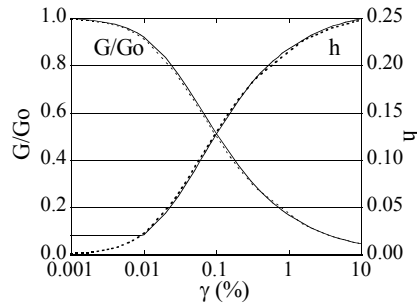
Fig.3 Investigation model

Fig. 4 Dynamic deformation characteristics of soil for investigations

one dimensional seismic response analyses are carried out using a multi degree of freedom system model.

3.1 Analysis conditions

The soil model consists of the two layers as shown in Fig. 3 The surface layer is a nonlinear clayey soil and divided into elements (sub-layers). The viscous boundary of the bedrock (the lower layer) properties is set at the bottom of the lowest element. The SHAKE and the R-O models are used for the comparison as the conventional models.

Fig. 4 shows the dynamic deformation characteristics of the clayey soil of the surface layer used in this analysis. As for the R-O model, the dynamic deformation characteristics are set as h_{max} =26% and γ=0.1% at G/G_0=0.5 (See Fig. 4).

The focused frequency ranges of the causal hysteretic damping model are set to 0~10 Hz which are equivalent to the values in the previous chapter.

El Centro 1940 NS wave (time step: 0.02 s, duration: 53.76 s) is used as the input ground motion. The maximum acceleration of the input motion is set at three levels (100 Gal, 500 Gal and 900 Gal). They are defined as $2E$ (two times of the upward wave) at the top of the bedrock where the viscous boundary is placed.

With regard to the proposed and the R-O models, the value for Δt in the analysis is set at 0.005 s. The Newmark-β method ($\beta = 1/4$) is used for the time integral method, and the modified Newton - Raphson method is employed in the convergence calculation. In the frequency response analysis using the SHAKE model, the frequency range is up to 25 Hz and $\Delta f = 0.0122$ Hz. The value of α (ratio of the effective strain to the maximum strain) used in the equivalent linear analysis is set to 0.65.

3.2 Comparison of response behavior

First, the characteristics of the proposed model are compared with that of the R-O model using one - element model. The sinusoidal strain wave (1.0 Hz) with increasing amplitude until 0.015 is given. Fig. 5 shows the shear stress (τ) vs. shear strain (γ) relation of both models. Their
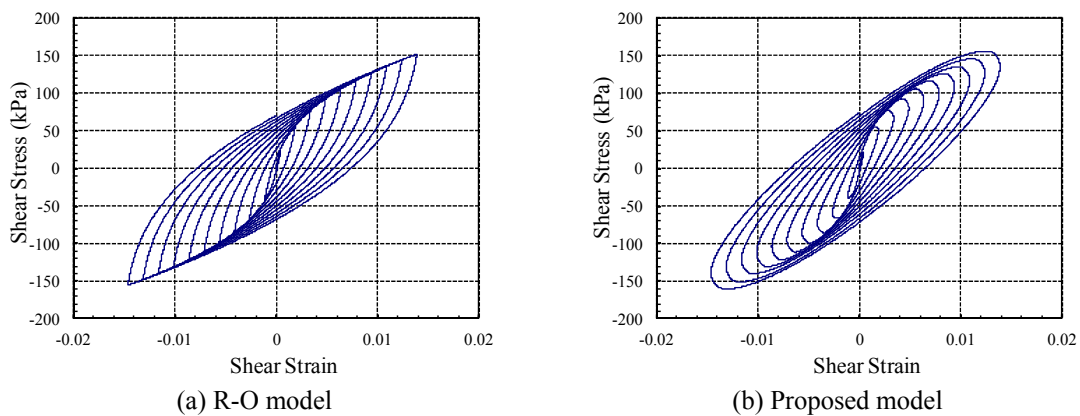

(a) R-O model   (b) Proposed model
Fig. 5 Comparison of stress-strain relationship of one element

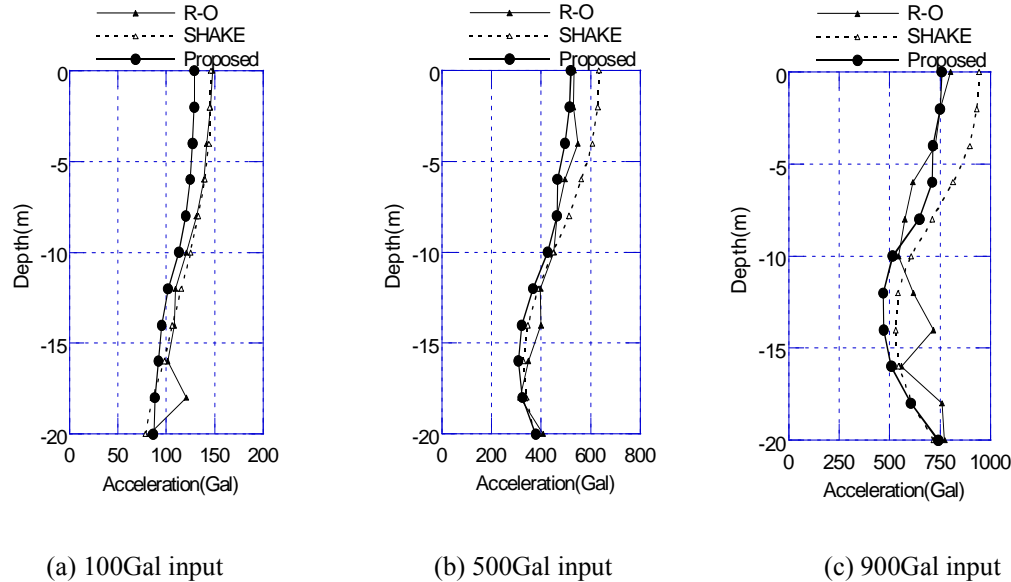(a) 100Gal input   (b) 500Gal input   (c) 900Gal input
Fig. 6 Comparison in maximum response acceleration

characteristics of are similar, but the shapes slightly differ. The R-O model shows spindle shapes whereas the proposed model shows oval shapes.

Subsequently, the proposed model is compared with the R-O and the SHAKE models with regard to the response behavior. In this section, the division of the surface layer is set to be 10.

Fig. 6 compares the maximum acceleration values in the cases of 100 Gal, 500 Gal and 900 Gal for the input ground motion. The maximum acceleration of the proposed model is slightly smaller than that of the R-O and the SHAKE models in the case of 100 Gal input (approximately 12% at the ground surface position). However, with an increase in the input level, the maximum acceleration of the proposed model shows almost the same value as that of the R-O model. On the other hand, the maximum acceleration of the SHAKE model becomes larger than that of the other two models in the cases of 500 Gal and 900 Gal input level. It is thought that this difference in the SHAKE model is caused by the overestimating the response owing to $\alpha = 0.65$. The response profile for the R-O model shows a large uneven shape in the vertical direction. In contrast, the response profile for the proposed model results in a relatively smooth continuous shape, similar to the SHAKE model. This is also discussed in section 3.3.

Fig. 7 illustrates the comparison in the maximum response displacement. The results of the SHAKE model are smaller than those of the R-O model in all cases and parts. The results of the proposed model are in between those of these two models; similar to those of the SHAKE model in the case of the input level being small (100 Gal), and close to those of the R-O model in the case of the input level being large (900 Gal).

The comparisons for the maximum response shear strain are shown in Fig. 8. In the same manner as that of the maximum response displacement, the maximum response shear strain of the SHAKE model is smaller than that of the R-O model in almost all cases and parts. Both results almost match. However, in the cases of 500 Gal and 900 Gal inputs, the difference between both models increases at their lower parts with large strain. It is thought that this happens because the
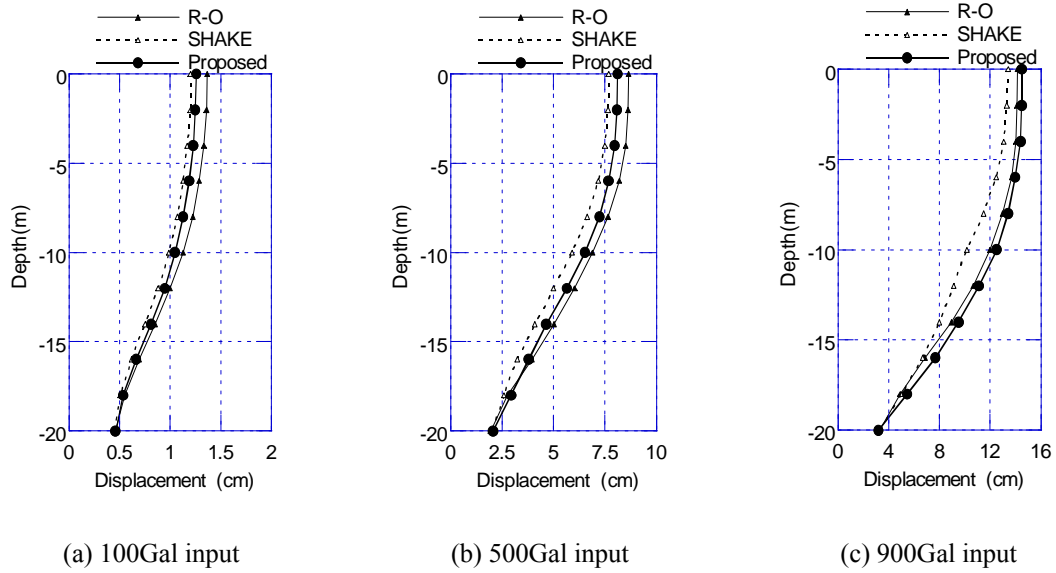
(a) 100Gal input   (b) 500Gal input   (c) 900Gal input

Fig. 7 Comparison in maximum response displacement

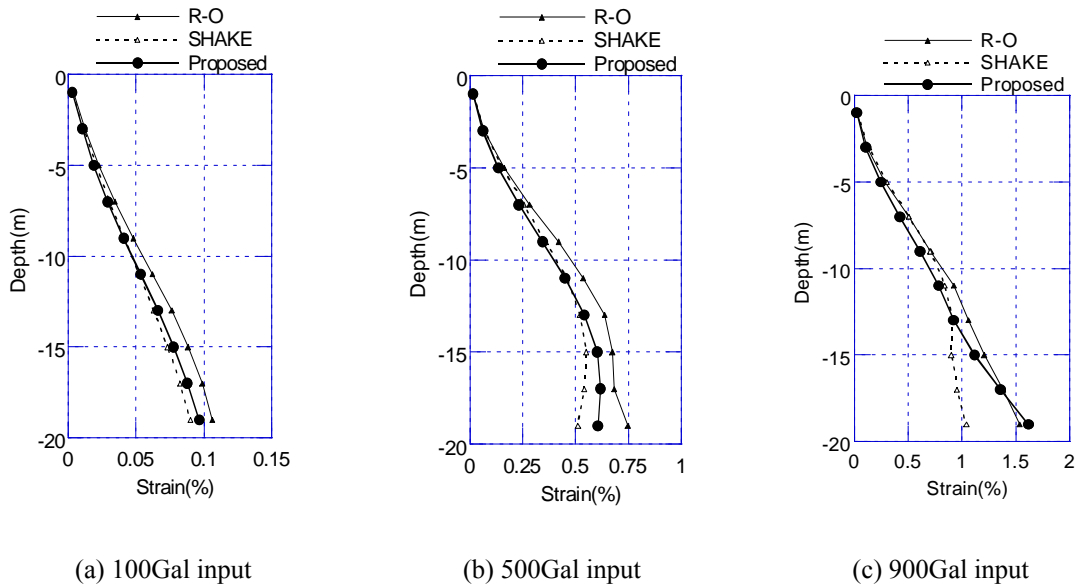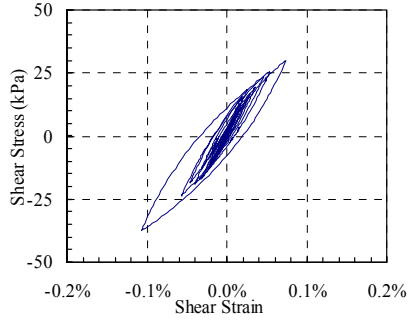(a) 100Gal input   (b) 500Gal input   (c) 900Gal input

Fig. 8 Comparison in maximum response shear strain

accuracy of the SHAKE model decreases as the strain increases. Overall, the results of the proposed model are close to the SHAKE model. However, at the lower parts where the strain is large, the results of the proposed model approach those of the R-O model rather than those of the SHAKE model, following an increase in the input level.

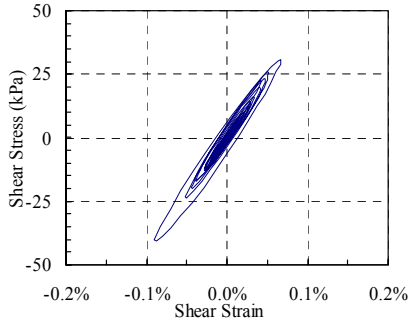Figs. 9(a)-(f) indicate the stress–strain relation of the elements at the lowest parts of the R-O,
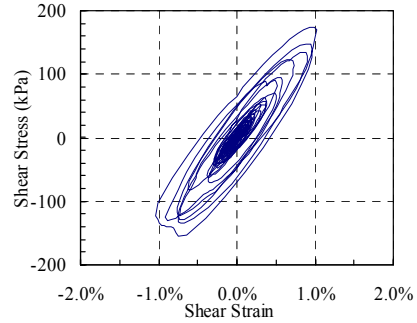
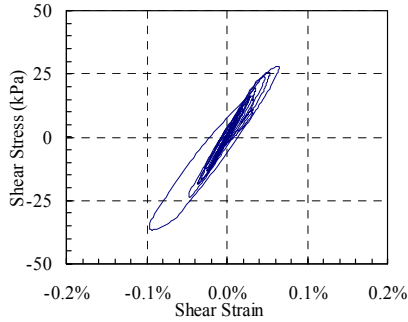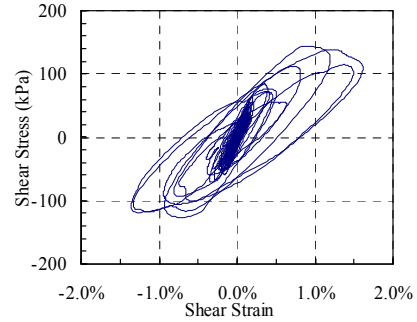(a) R-O model (100Gal input)
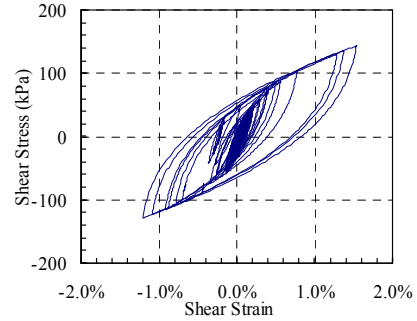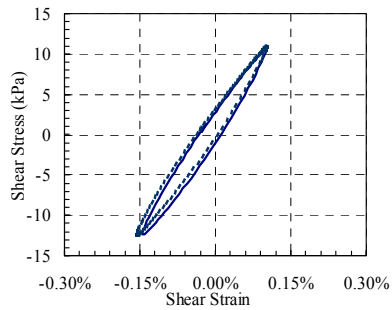
(b) R-O model (900Gal input)
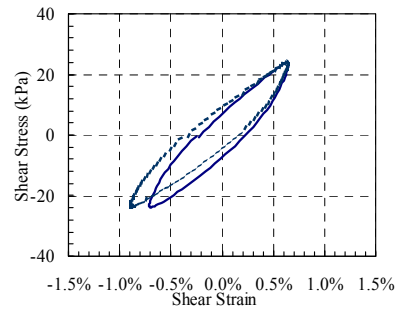
(c) SHAKE (100Gal input)

(d) SHAKE (900Gal input)

(e) Proposed model (100Gal input)

(f) Proposed model (900Gal input)

(g) Cyclic tri-axial test（$\gamma \approx 0.15\%$）

(h) Cyclic tri-axial test（$\gamma \approx 1.0\%$）

Fig. 9 Comparison in stress-strain relation between conventional models and proposed model

the SHAKE, and the proposed models. The results obtained from 0 s to 30 s for all models in the case of 100 Gal and 900 Gal inputs are shown. As for the proposed model, the secant stiffness decreases and the shape of the loop becomes thick according to an increase of the strain level. The shape of the loop for the proposed model corresponds relatively well to that of the R-O model.

In general, in the analysis of the SHAKE model, the output shear stress τ does not consider damping. The value for τ in Fig. 9 was obtained from the inverse Fourier transform by calculating τ, considering the damping in the frequency domain and using the final convergent value shown in Table 1. Although the results of the SHAKE model correspond fairly well to those obtained from other models, the loop shape is slightly more slender and the secant stiffness is higher to some degree. This tendency is conspicuous in the case of the 900 Gal input as shown in Fig. 9(d).

Figs. 9(g) and (h) show the stress–strain relation of the silt clay (initial $V_s = 102$ m/s) obtained from cyclic triaxial tests as an example of actual soil data. Each figure shows the loop shapes at the 5th and 10th cyclic loading, where the maximum shear strain reaches about 0.15% and 1%, respectively.

The elliptical loop shape with slightly sharp ends obtained from the test corresponds well to those of the R-O and the SHAKE models. It can be said that the elliptical loop shape with a comparatively rounded point for the proposed model is also nearly equivalent to the test results.

Fig. 10 illustrates the comparison in the acceleration response waves (0-10 s) at the ground surface positions between the proposed and the R-O models. The comparison between the proposed and the SHAKE models is indicated in Fig. 11. All comparisons are carried out in the cases of 100 Gal and 900 Gal inputs. Although the waves of the proposed model correspond well
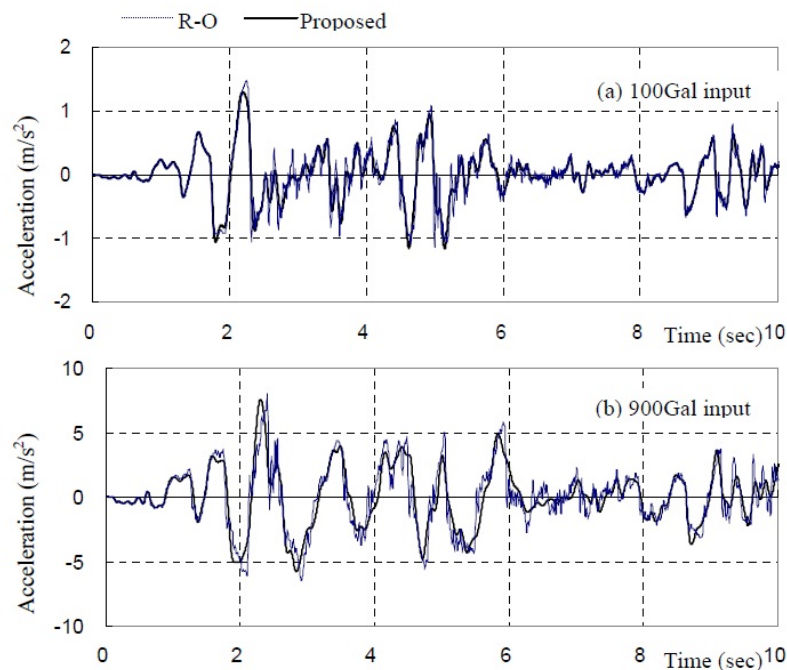

Fig. 10 Comparison in acceleration wave between proposed model and R-O model

Table 1 Shear modulus (G/G_0) and damping ratio (h) used in SHAKE analysis

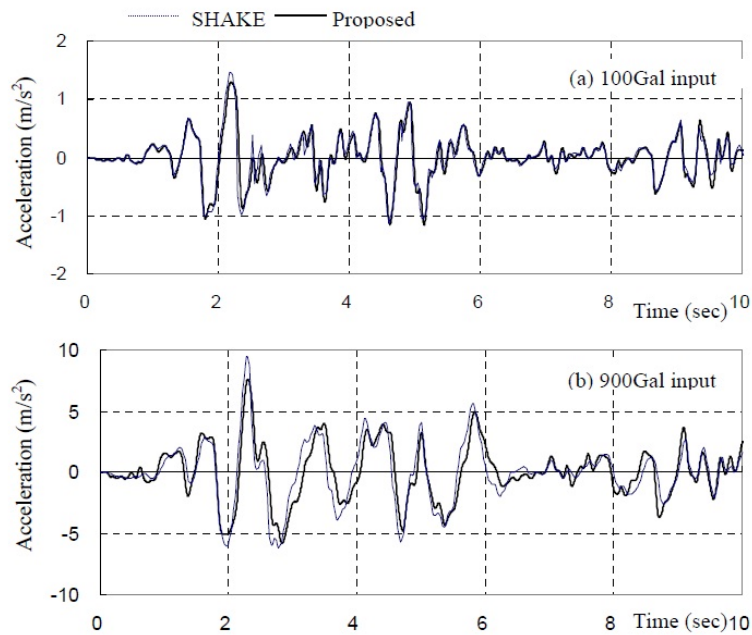| Input	Effective strain (%)	G/G_0	h (%)
100 Gal	0.059	0.635	9.6
900 Gal	0.676	0.207	20.8

Fig.11 Comparison in acceleration wave between proposed model and SHAKE

to those of the R-O model as a whole, fine waves with high frequency are seen more in the R-O model than the proposed model.

The acceleration response wave of the proposed model nearly corresponds to that of the SHAKE model in the case of the 100 Gal input. In the case of 900 Gal input, a difference is discernible between these two models. The results of the SHAKE model are larger in the peak with 2-3 s and smaller in the peak with 8-9 s than those of the proposed model. It is thought that this happens because the same damping ratio was used for the SHAKE model in all frequency ranges and analysis periods.

It was confirmed from the above that the response behavior of the proposed model corresponds fairly well to that of the R-O model and the results of the soil test.

However, the above tendencies may not be the same because of soil conditions or input ground motion behavior. Therefore, further investigations need to be carried out considering the variations in the analysis conditions.
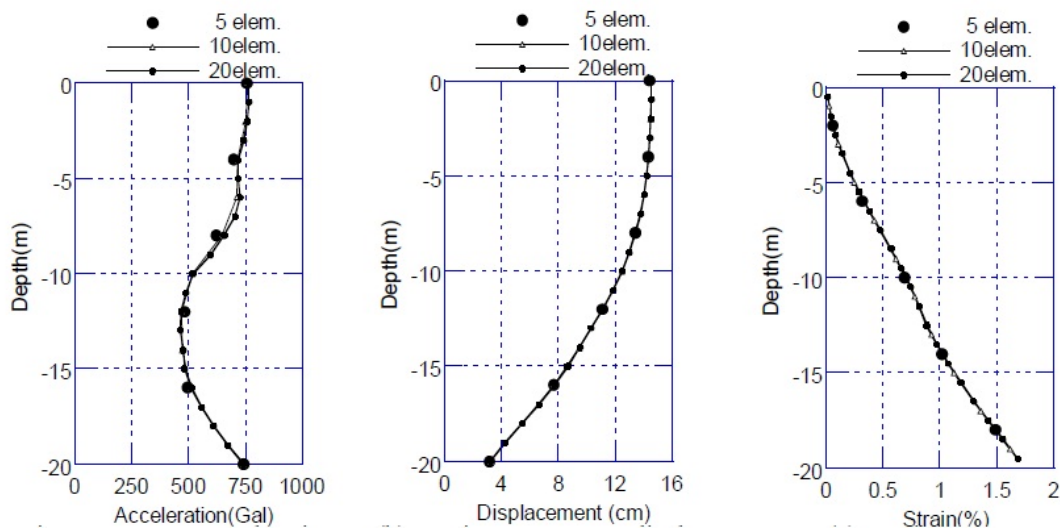
3.3 Effects of element division

The effects of the soil model shown in Fig. 3, regarding the response when changing the element division of the surface layer, are investigated. For 900 Gal input, the response values in the cases where the surface layer is divided into 5 and 20 elements, in addition to the case of 10 elements, are calculated. The analysis conditions except for the element division are the same as those in the foregoing section.

The comparison of the response behavior is carried out between the proposed and the R-O
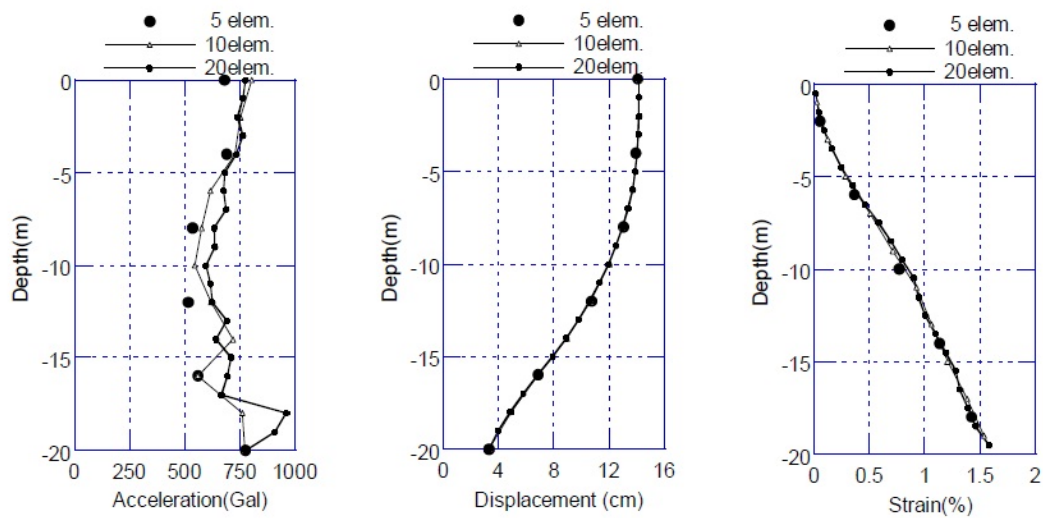
(a)Maximum response acceleration   (b) Maximum response displacement   (c) Maximum response shear strain
Fig.12 Study on effects of element division (R-O model)

(a) Maximum response acceleration   (b) Maximum response displacement   (c) Maximum response shear strain
Fig. 13 Study on effects of element division (Proposed model)

models. Fig. 12 shows the maximum response value of the R-O model. The effects of the element division on the maximum response displacement (Fig. (b)) and the maximum response shear force (Fig. (c)) are small. The values continuously change in all element divisions. On the other hand, the values of the maximum response acceleration (Fig. (a)) show uneven shapes, and differences are discernible in each case.

As for the proposed model, the maximum response values continuously vary in Fig. 13 and the differences in the response value caused by the element division are small. Under the conditions of this investigation, the maximum response values are thought to continuously change. Therefore, it can be thought that the behavior of the proposed model is more desirable.

4. Study on the controlling parameters

In this chapter, the following two parameters are investigated:
  (1) Time to define the time delay component
  (2) Memory time for the maximum strain
They may not be common in time history analysis, but play an important role in the proposed analyses. Thus, these two parameters are described and their effect on the response results is studied.

These same parameters were used in (Nakamura 2007). In this paper, the first parameter was studied, while the second parameter was set constant.

4.1 Effects of time to define the time delay component

In the proposed model, the time delay component exists only in the stiffness terms (k_j) of the impulse response as shown in Eqs. (3) and (5). The time delay components are thought as coefficients indicating the effects of the past state at the time $t - t_j$ (where $t_j = j\Delta t$) upon the present state at t. In this paper, the impulse response is thought to vary with time, so the time delay component k_j also varies between time $t - t_j$ and t. Hereafter, they are distinguished by the notations $k_j(t - t_j)$ and $k_j(t)$.

There is a problem in determining the values that should be used as the time delay components k_j in order to calculate the reaction at the present time as indicated in Eq. (5) from among $k_j(t - t_j)$, $k_j(t)$, and others. Strictly speaking, k_j is affected by variations in soil properties during this period [from $(t - t_j)$ to t], so it is explained by Eq. (8) using the weight coefficient $A(t)$.

$$k_j = \int_{t-t_j}^{t} A(\tau) k_j(\tau)/t_j \, d\tau \qquad Where \int_{t-t_j}^{t} A(\tau) \, d\tau = 1 \qquad (8)$$

However, it is not easy to determine $A(\tau)$ because it may not be the same function at various conditions and may vary as a function of the analysis conditions. Therefore, parameter surveys are carried out for the three cases shown in Table 2 as representative methods.

In cases 1 and 3, values at both ends of the period from $(t - t_j)$ to t are used. Accordingly, assuming that k_j monotonously varies during this period [from $(t - t_j)$ to t], it can be thought that an upper as well as a lower limit values can be provided. Case 2 indicates an intermediate value where k_j linearly varies during this period and the value for $A(\tau)$ is constant.

If the difference in the response result between each case is small, it has small effect on this
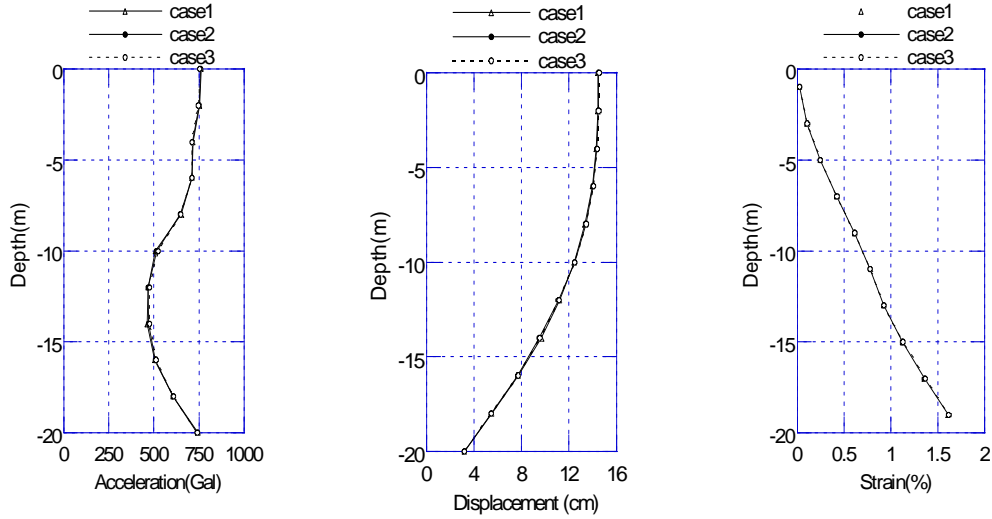
(a) Maximum response acceleration   (b) Maximum response displacement   (c) Maximum response shear strain
Fig. 14 Effects of definition of time delay components on maximum response value
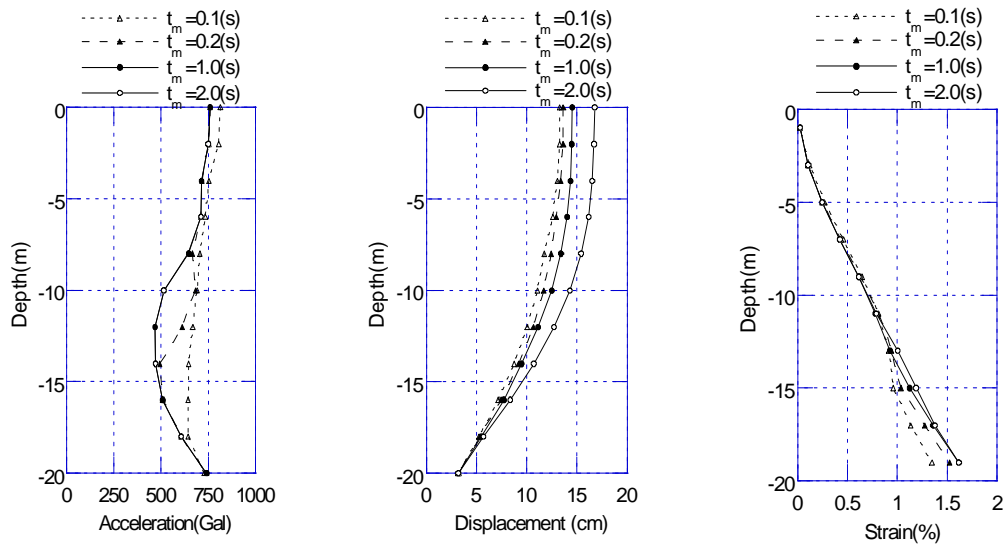
(a) Maximum response acceleration   (b) Maximum response displacement   (c) Maximum response shear strain
Fig. 15 Effects of memory time of maximum strain on maximum response value

problem. Therefore, the results in all cases are thought to be almost valid for the problem. In the analysis in chapter 3, case 2 was applied.

In this section, for cases 1–3 where 900 Gal is input, analyses are carried out and the results are compared with each other. Fig. 14 illustrates the comparison in the maximum response value

Table 2 Definition of k_j

	Time delay component k_j
Case 1	$k_j (t - t_j)$
Case 2	$(k_j (t - t_j) + k_j (t)) / 2$
Case 3	$k_j (t)$

(a) $t_m = 0.1$(sec)

(b) $t_m = 0.2$ (sec)

(c) $t_m = 1.0$ (sec)
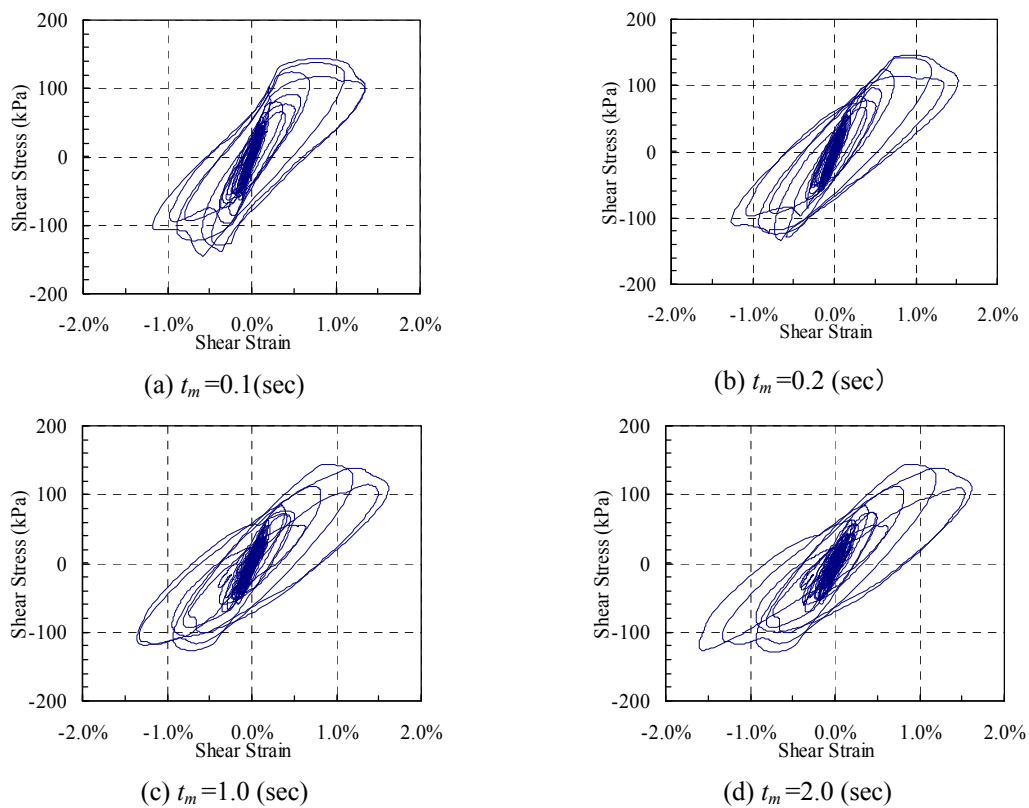
(d) $t_m = 2.0$ (sec)

Fig. 16 Effects of memory time for maximum strain stress-strain

for each case. Differences between these three cases can hardly be seen in any figure. From this, it is confirmed that the effects of the problems mentioned above are insignificant.

4.2 Effect of memory time of the maximum strain

The strain value of each element in the soil model greatly fluctuates each time. To some degree, when considering actual materials with strain dependency, it can be thought that the materials are affected by the maximum strain experienced in the past, but they are not dealt with instantly, only for the strain value at each time. For example, in cases where the shear strain changes from a large

value to zero, it is difficult to expect that the characteristics of the materials also return to the initial value instantly. In particular, the impulse response used in the proposed method conveys the effects of the past to the present states. From this point of view, the effects of the maximum strain in the past state cannot be neglected.

Accordingly, how to consider the effects of maximum strain in the past state is a subject to note. In particular, this must be established according to actual experimental data. However, it has yet to be made clear.

In this section, investigations using the memory time (hereafter referred to as t_m) as a parameter are carried out. Fig. 15 illustrates the comparison in the maximum response value in the cases of t_m being set at 0.1, 0.2, 1.0 and 2.0 s. The input ground motion is set at 900 Gal.

Fig (a) related to the maximum response acceleration shows that the response value increases as the value for t_m decreases. In the cases of 1.0 s and 2.0 s, the differences in the response are insignificant. However, in the case of 0.2 s or less, the response in the center of the surface layer increases. In contrast, Fig (b) shows that for the maximum response displacement the response increases with a rise in t_m. In the case of 0.1–1.0 s for t_m, the differences in the response are relatively small, but in the case of 2.0 s, the differences slightly increase. In Fig. (c), for the maximum response shear strain, the differences are shown to be fairly small.

Fig. 16 illustrates the stress–strain relation of the elements at the lowest parts of the surface layer in the aforementioned cases. It is clear that with an increase in the value for t_m, the loop shows an elliptical shape and its secant stiffness decreases. On the other hand, in the case of small t_m, the loop is close to a rectangle and its secant stiffness becomes large.

It can be inferred that the above characteristics are caused by the fact that with the increase in the value for t_m, it took longer to estimate the strain level to a high degree and as a result G/G_0 was estimated to be lower and h was estimated to be higher.

Although t_m is considered a useful parameter for controlling the loop shape in the analyses, it is desired that t_m should originally be established based on the data obtained from the experiments. From this point of view, the accumulation of data in the future is thought to be important.

5. Study on the effects of frequency dependency on responses

The key characteristics of the proposed method are the frequency and the strain dependencies of the model.

In the previous chapter, the frequency dependency was dealt as frequency independency (constant value in focused frequency ranges). In this chapter, the effect of the frequency dependency upon responses is investigated using a model in which the damping ratio h decreases along with the frequency.

It is indicated that the frequency dependency of the damping is observed in the actual soil deposit. The investigation in this chapter aims at quantitatively confirming that both the frequency and the strain dependencies of the proposed model are affected by the response results.

5.1 Establishment of negative gradient damping model

In order for the imaginary part to be constant in the focused frequency range ($0 \leq \omega \leq \omega_m$), the
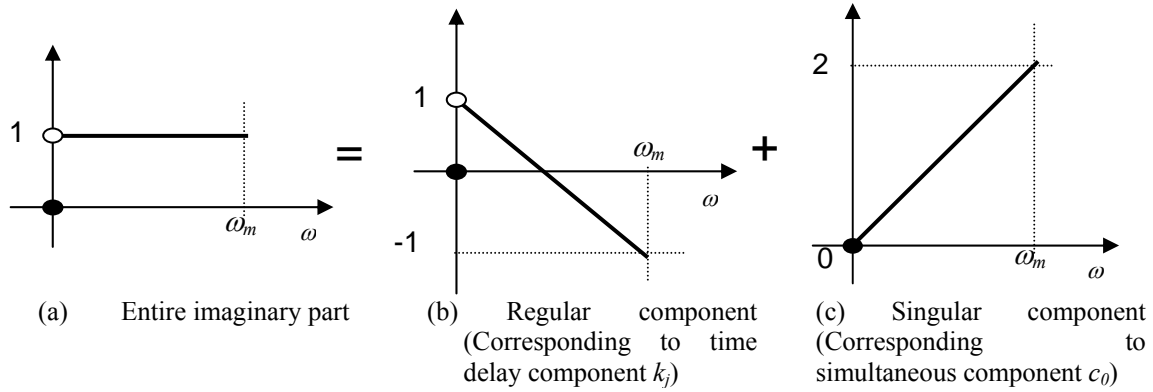
Fig. 17 Imaginary part of unit imaginary function model (constant gradient model)

causal unit imaginary function $Z'(\omega)$ used in the causal hysteretic damping model is modeled as shown in Fig. 17(a). This can be indicated as the sum of the regular component of the negative gradient (Fig. 17(b)) and the singular component (Fig. 17(c)). See Ref. 11 for details.

In this chapter, the imaginary part is modified to have a negative gradient in the focused frequency range as $Z'(\omega) = 1$ and $Z'(\omega_m) = 0$ as shown in Fig. 18(a). The regular component as seen in Fig. 18(b) is not changed, but the gradient of the singular component as seen in Fig. 18(c) is changed to 1/2. Hereafter, this model is called the negative gradient model and that shown in Fig. 17 is called the constant gradient model. The causal real part of the negative gradient model is same as that of the constant gradient model because the causality condition is not affected by the singular component. As a result, the impulse response of the negative gradient model obtained from the transform to the time domain is also similar to the impulse response of the constant gradient model. The impedance $Z'_m(\omega)$ of the negative gradient model and the reaction $z'_m(t)$ in the time domain can be described by Eqs. (9) and (10), respectively, using the calculated impulse response. From the comparison of these with the impedance $Z'(\omega)$ of the constant gradient model and the reaction $z'(t)$ in the time domain (see Eqs. (3) and (5)), it is made clear that the only
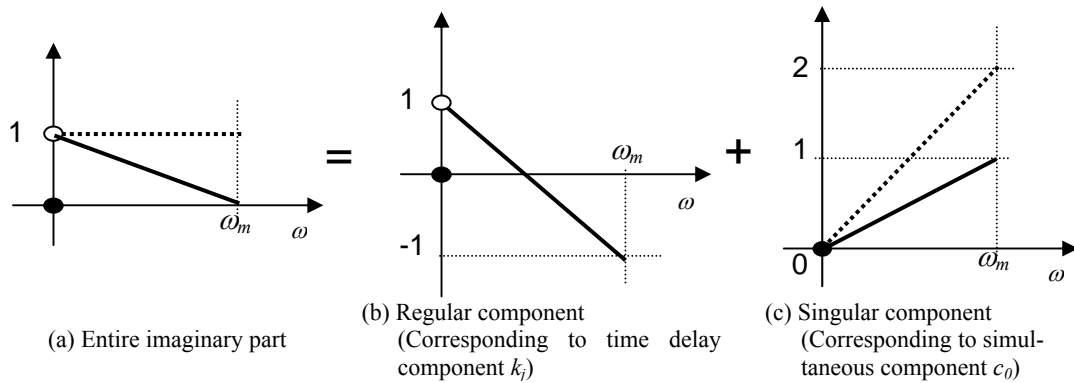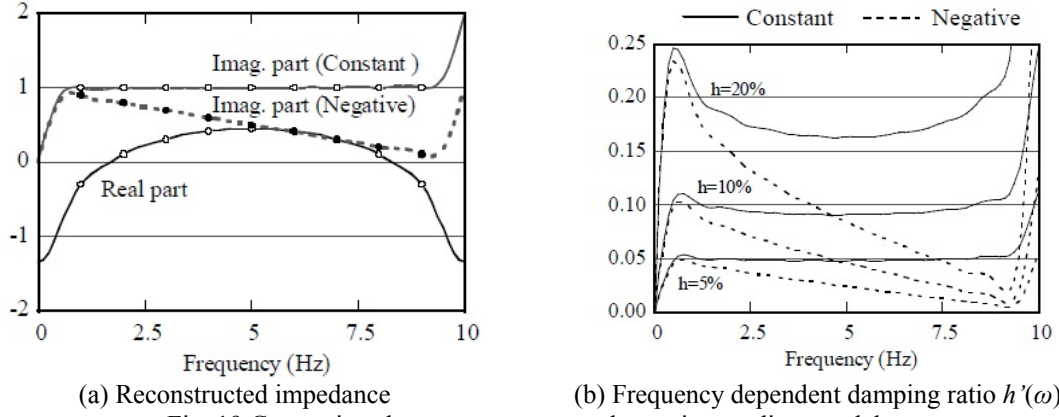

Fig. 18 Imaginary part of negative gradient imaginary function model (Broken line: constant gradient model)

(a) Reconstructed impedance   (b) Frequency dependent damping ratio $h'(\omega)$

Fig. 19 Comparison between constant and negative gradient model

difference is the coefficient (1/2) of the simultaneous component c_0 of the damping term whereas the time delay components are identical to each other.

$$Z'_m(\omega) = \frac{1}{2}i\omega \cdot c_0 + \sum_{j=1}^{n} k_j \cdot e^{-i\omega t_j} \tag{9}$$

$$z_m'(t) = \frac{1}{2}c_0 \cdot \dot{u}(t) + \sum_{j=1}^{n} k_j \cdot u(t - t_j) \tag{10}$$

Fig. 19(a) illustrates the impedance of the negative gradient and the constant gradient models recovered from the impulse response. Black and white circle marks show the data points used for the transform to the time domain.

The complex stiffness $S_m(\omega)$ including the negative gradient model can be indicated by substituting $Z'_m(\omega)$ for $Z'(\omega)$ of $S(\omega)$ shown in Eq. (1). The damping ratio $h'(\omega)$, which varies depending on the frequency, is expressed by using Eq. (11).

$$h'(\omega) = \sin\left(\frac{1}{2}\tan^{-1}\frac{\mathrm{Im}(S'_1(\omega))}{\mathrm{Re}(S'_1(\omega))}\right) \tag{11}$$

Fig. 19(b) compares the damping ratio $h'(\omega)$ of the negative gradient model obtained from Eq. (11) in the cases of $h = 5\%$, 10% and 20% with that of the constant gradient model.

The gradient of the proposed model can arbitrarily be varied by changing the coefficient of c_0 (hereafter referred to as C_m). However, since the high frequency components of the imaginary part become negative in the case of $C_m < 1/2$, the value in this case easily causes divergence in the time history response analyses. In the case of $C_m > 1$, the imaginary part has a positive gradient in the frequency.

5.2 Comparison of the response behavior

Fig. 20 shows the comparison in the maximum response value in the case of the 100 Gal input
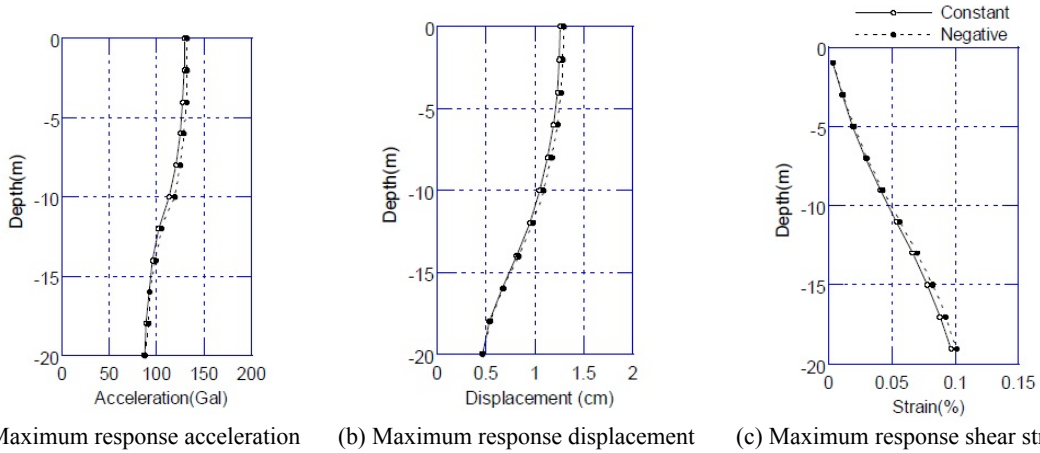
(a) Maximum response acceleration   (b) Maximum response displacement   (c) Maximum response shear strain

Fig. 20 Comparison in maximum response value between constant and negative gradient model (100Gal input)
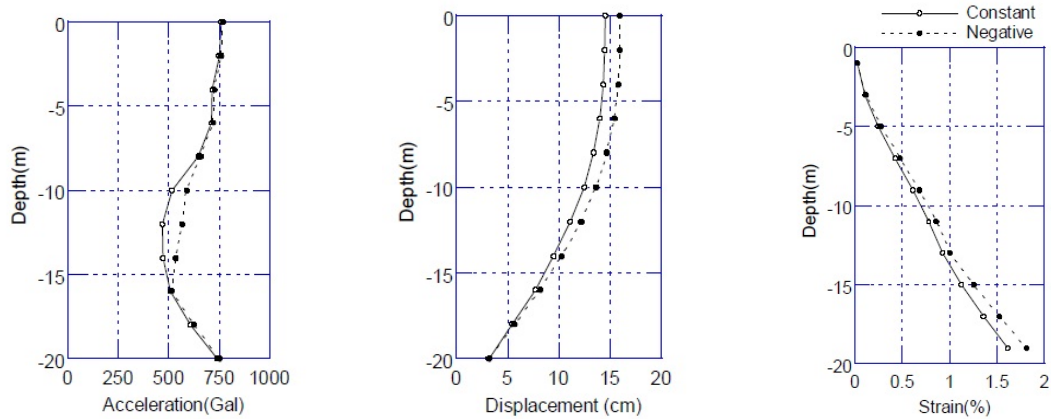
(a) Maximum response acceleration   (b) Maximum response displacement   (c) Maximum response shear strain

Fig. 21 Comparison in maximum response value between constant and negative gradient model (900Gal input)

between the constant gradient and the negative gradient models. The response results of both models almost match as shown in Fig. 20. However, the response value of the negative gradient model is slightly larger than that of the constant gradient model. It is thought that this is because the damping quantity of the negative gradient model is overall small. Fig. 21 shows the comparison in the maximum response value between these two models in the case of 900 Gal input. Compared with the case of the 100 Gal input, the differences in the response value between both models increases.

Fig. 22 shows the transfer functions in the cases of the 100 Gal and 900 Gal inputs obtained by dividing the response acceleration at the ground surface position by the input ground motion. For

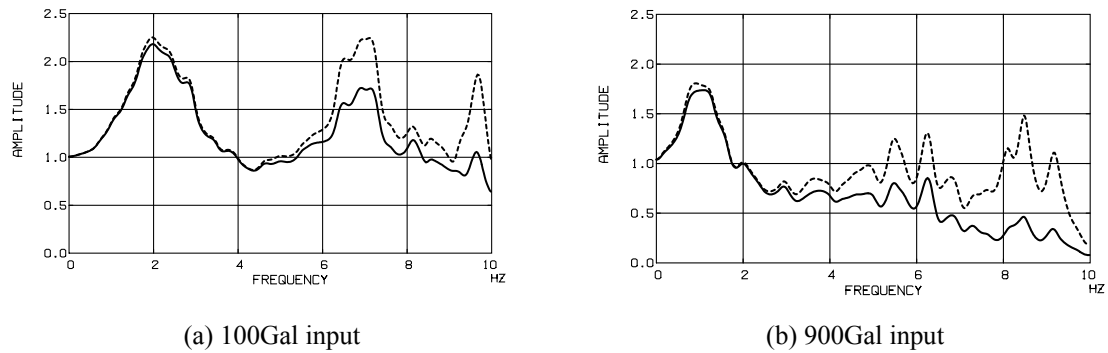(a) 100Gal input   (b) 900Gal input
Fig. 22 Comparison in transfer function (Acceleration on ground surface/Input ground motion)
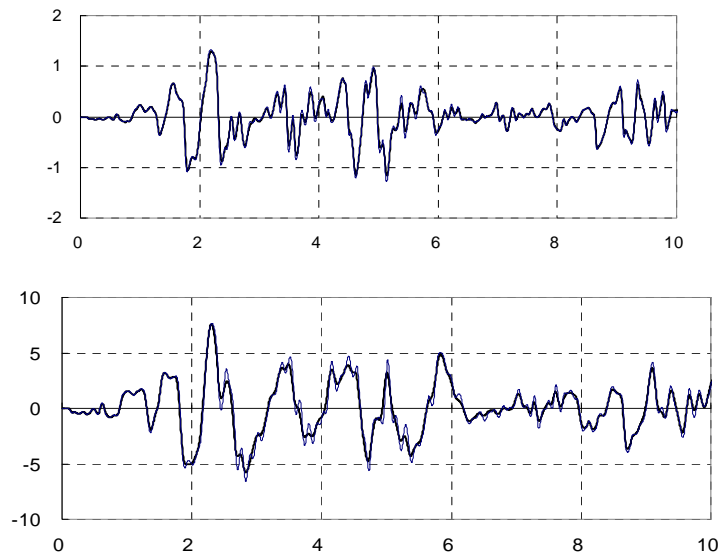
Fig. 23 Comparison in response acceleration wave at ground surface positions

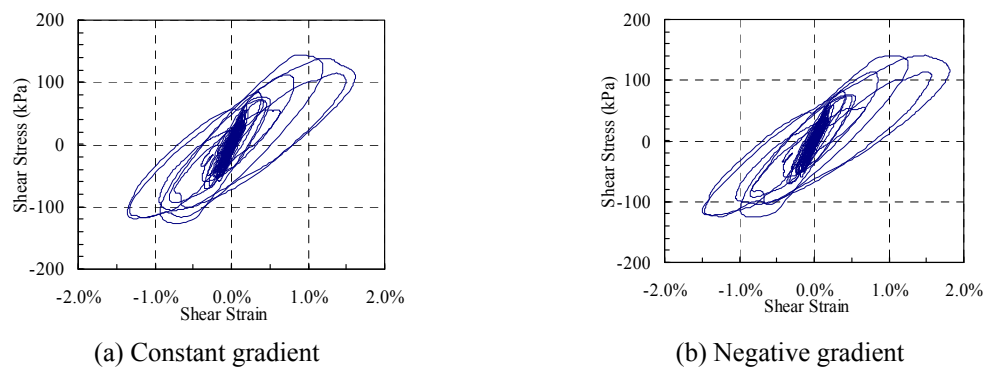(a) Constant gradient   (b) Negative gradient
Fig. 24 Comparison in stress-strain relation (900Gal input)

the sake of smoothing, the Parzen window with a bandwidth of 0.4 Hz is used. Both Figs. (a) and (b) show that in the high frequency regions the response of the negative gradient model is larger than that of the constant gradient model. It is thought that this is caused by the difference in the damping behavior between these two models. Compared with Fig. (a), in Fig. (b) the difference in the transfer function between both models is observed from a lower frequency region in the vicinity of 3 Hz and it also becomes larger. It is thought that this result contributes to the difference in the maximum response value shown in Fig. 21.

Fig. 23 illustrates the response acceleration waves of both models at the ground surface positions in the cases of 100 Gal and 900 Gal inputs. In Fig. (a), the difference between both models is small, but Fig. (b) shows the sharp and high peak point of the amplitude for the negative gradient model. It is thought that this happens because the models in the cases of the 900 Gal input contain a large number of high frequency components due to the stronger nonlinearity.

Fig. 24 compares the stress–strain relation in the case of the 900 Gal input between both models. It can be said that the difference between both models is overall small. However, the negative gradient model shows a slightly more slender shape than the constant gradient model. This may be caused by the fact that the damping quantity of the negative gradient model is smaller than that of the constant gradient model.

6. Conclusions

This paper studied the applicability of the causal hysteretic damping model to nonlinear analyses. First, the response behavior of the proposed model was investigated through seismic response analyses using a two-layered soil model. It was confirmed that the response behavior of the proposed model corresponds fairly well to that of the R-O model and the results obtained from soil tests.

Furthermore, the investigations related to the effects of the element division resulted in showing that the proposed model has more stable characteristics, which are not easily affected by the element division, than the R-O model.

From the results of the investigations of the characteristic parameters used in the response analysis of the proposed model, it was indicated that the appropriate establishment of these parameters is important because the memory time of the maximum strain affects the loop shape in the stress-strain relation and changes the response behavior. Moreover, using the key characteristic of the proposed method, the frequency dependency can be directly prescribed, a simple model which can decrease the damping ratio depending on the frequency was established. Subsequently, it was confirmed that the response behavior is favorably affected by the frequency dependency using this simple model.

From these results, the characteristics of this proposed model can be indicated as follows:

(1) The proposed model can cope with any arbitrary strain dependency (G-γ, h-γ relation). It is not limited to shapes such as those of the R-O or the hyperbolic model.
(2) The frequency dependency can be defined with a direct form. For example, the damping ratio of the model can be set to be constant or negative gradient for the frequency.
(3) The concept of the model is so simple that any hysteresis rule such as a skeleton curve or a Masing rule is unnecessary.
(4) Compared with the R-O model, the behavior of the proposed model is not easily affected by the element division.

(5) By using the memory time of the maximum strain as a parameter, the shape of the hysteresis loop can be changed to some degree.

References

Hardin, B.O. and Drnevich, V.P. (1972), "Shear modulus and damping in soils: Design equations and curves", *J. SMFD, proc., ASCE*, **98**(7), 667-692.

Jennings, P.C. (1963), "Periodic response of a general yielding structure", *Proc. ASCE*, **90**(2), 131-166.

Kausel, E. and Assimaki, D. (2002), "Seismic simulation of inelastic soils via frequency-dependent moduli and damping", *J. Eng. Mech.-ASCE*, **128**(1), 34-47.

Kumazaki, I. (1998), "Hysteresis model considering shear-strain dependency of fractal dimension and momentary deformation modulus", *Proceedings of International Association for Mathematical Geology*, 602-607.

Masing, G. (1926), "Eigenspannungen und verfestigung being messing", *Proc. 2nd int. Congress of Applied Mechanics,* Zurich, Switzerland, 332-335.

Nakamura, N. (2006a), "A practical method to transform frequency dependent impedance to time domain", *Earthq. Eng. Struct. D.*, **35**(2), 217-234.

Nakamura, N. (2006b), "Improved methods to transform frequency dependent complex stiffness to time domain", *Earthq. Eng. Struct. D.*, **35**(8), 1037-1050.

Nakamura, N. (2007), "Practical causal hysteretic damping", *Earthq. Eng. Struct. D.*, **36**(5), 597-617.

Nakamura, N. (2008a), "Transform methods for frequency dependent complex stiffness to time domain using real or imaginary data only", *Earthq. Eng. Struct. D.,* **37**(4), 495-515.

Nakamura, N. (2008b), "Nonlinear response analysis considering dynamic stiffness with both frequency and strain dependencies", *J. Eng. Mech.-ASCE*, **134**(4), 530-541.

Sato, T., Fushimi, M. and Tatsumi, Y. (2001), "Inversion of strain-dependent nonlinear characteristics of soil using weak and strong motions observed by borehole sites in japan", *B. Seismol. Soc. Am.*, **91**(2), 365-380.

Schnabel, P.B., Lysmer, J. and Seed, H.B. (1972), "SHAKE A computer program for earthquake response analysis of horizontally layered sites", Report No.EERC72-12, University of California, Berkeley.

Yoshida, N., Kobayashi, S., Suetomi, I. and Miura, K. (2002), "Equivalent linear method considering frequency dependent characteristics of stiffness and damping", *Soil Dyn. Earthq. Eng.*, **22**, 205-222.

IT